Measuring The Tensile Strain of Wood By Visible And Near-Infrared Spatially Resolved Spectroscopy

Ma Te (mate@agr.nagoya-u.ac.jp)
Nagoya Daigaku Daigakuin Seimei Nogaku Kenkyuka Nogakubu
Tetsuya Inagaki
Nagoya University: Nagoya Daigaku
Masato Yoshida
Nagoya University: Nagoya Daigaku
Mayumi Ichino
Nagoya University: Nagoya Daigaku
Satoru Tsuchikawa
Nagoya University: Nagoya Daigaku

Research Article

Keywords: Tensile strain of wood, non-destructive evaluation, spatially resolved spectroscopy, visible and short-wave light scattering, multivariate analysis

Posted Date: June 17th, 2021

DOI: https://doi.org/10.21203/rs.3.rs-570550/v1

Measuring the Tensile Strain of Wood by Visible and Near-Infrared Spatially Resolved Spectroscopy

---

Te Ma, Tetsuya Inagaki, Masato Yoshida, Mayumi Ichino, and Satoru Tsuchikawa*

***Corresponding author: Satoru Tsuchikawa,** Graduate School of Bioagricultural Sciences, Nagoya University, Furo-Cho, Chikusa, Nagoya 464-8601, Japan, Email addresses: st3842@agr.nagoya-u.ac.jp

Te Ma (mate@agr.nagoya-u.ac.jp), Tetsuya Inagaki (inatetsu@agr.nagoya-u.ac.jp), Masato Yoshida (yoshida@agr.nagoya-u.ac.jp), and Mayumi Ichino (ichino.mayumi@j.mbox.nagoya-u.ac.jp): Graduate School of Bioagricultural Sciences, Nagoya University, Furo-Cho, Chikusa, Nagoya 464-8601, Japan.

Declarations:

Funding: This study is supportted by JSPS (KAKENHI, no.19K15886)

Conflicts of interest/Competing interests: Not applicable

Availability of data and material: Yes

Code availability: Not applicable

Authors' contributions:

Te Ma: methodology, data collection and analysis, writing-original draft preparation

Tetsuya Inagaki: methodology, data validation, and writing- reviewing.

Masato Yoshida: contributed to capture the submicroscopic changes during tension testing, writing- reviewing

Mayumi Ichino: data collection and analysis

Satoru Tsuchikawa*: supervision, conceptualization, writing- reviewing and editing

Ehics approval: Not applicable

Consent to participate: Not applicable

Consent for publication: Not applicable

Abstract:

Wood has various mechanical properties, so stiffness evaluation is critical for quality management. Using conventional strain gauges constantly is high cost, also challenging to measure precious wood materials due to the use of strong adhesive. This study demonstrates the correlation between light scattering changes inside the wood cell walls and tensile strain. A multifiber-based visible-near-infrared (Vis–NIR) spatially resolved spectroscopy (SRS) system was designed to rapidly and conventiently acquire such light

scattering changes. For the preliminary experiment, samples with different thicknesses were measured to evaluate the influence of thickness. The differences in Vis–NIR SRS spectral data diminish with an increase in sample thickness, which suggests that the SRS method can successfully measure the whole strain (i.e., surface and inside) of wood samples. Then, for the primary experiment, 18 wood samples with the same thickness (2 mm) were tested to construct a strain calibration model. The prediction accuracy was characterized by a determination coefficient (R^2) of 0.86 with a root mean squared error (RMSE) of 297.89 με for five-fold cross-validation; for test validation, The prediction accuracy was characterized by an R^2 of 0.82 and an RMSE of 345.44 με.

Keywords:

Tensile strain of wood, non-destructive evaluation, spatially resolved spectroscopy, visible and short-wave light scattering, multivariate analysis

1. Introduction

Wood is a natural material with multi-layered elongated cells. Due to the variability of its mechanical properties, the stiffness evaluation of each structural wooden member is critical for quality management (Baillères et al. 2012; Montero et al. 2012). The wood

55 cell wall is a macromolecular composite formed of cellulose, hemicelluloses, and lignin
56 (Hon and Chang 1984). Cellulose is the primary component in bearing tensile stress
57 (Salmén and Bergström 2009). In contrast, hemicelluloses function as a coupling agent
58 to hold the cellulose (Burgert 2006). The conventional method for wood strain
59 measurement is to use a strain gauge, which is high cost (either disposable or reusable
60 ones) in constant use (Yang et al. 2005). In addition, it is challenging to measure precious
61 wood materials due to the use of a strong adhesive, which can destroy the wood after
62 removal. For example, the heritage community generally does not allow the application
63 of strain gauges on wooden arts (Anaf et al. 2020). Moreover, difficulties arise when strain
64 gauges are used in an environment where the electromagnetic wave interference is
65 extensive (Liu et al. 2015; Barr et al. 2017).
66
67 X-ray diffraction (Kamiyama et al. 2005) and infrared (IR) spectroscopy (Åkerholm
68 and Salmén 2001) can detect wood structure-function relationships at the nano- and
69 microstructural levels. Indeed, Raman spectroscopy (Hsieh et al. 2008) can predict
70 sample strains based on a typical shift peak at a wavenumber of 1095 cm^{-1}, which
71 corresponds to the glycosicdic bond in the cellulose structure backbone (Guo and Altaner
72 2018). Moreover, the band shift varies among specimens (Eichhorn 2001), and the

molecular strain is smaller than the macroscopic strain (Peura et al. 2007). In contrast, Near-IR (NIR) spectroscopy (wavelength: 800–2500 nm or wavenumber: 12500–4000 cm^{-1}) is well-suited for characterizing organic compounds in samples, mainly in combination with multivariate mathematical techniques. When NIR light illuminates and transmits through an object, the energy of the incident electromagnetic wave changes due to the stretching and bending vibrations of chemical bonds, such as O–H, N–H, and C–H. Subsequently, the quality and quantity of an object can be evaluated nondestructively, rapidly, and cost-effectively by analyzing the light reflectance and transmittance values (Ma et al. 2020). Compared with microtomed sections needed for IR spectroscopy, NIR spectroscopy can nondestructively measure wood samples up to several millimeter thick without special sample pretreatments (Salmén and Bergström 2009). This is essential when focusing on practical applications, as thin samples prepared in lab behave differently than solid wood, e.g., including stress relaxation in the former (Yu et al. 2009). Taking advantages of NIR spectroscopy, Guo et al. (2019) analyzed band shifts and band assignments on NIR light absorbance characteristics during the wood tension test, the results of which suggest that the observed band shifts correlate with wood tension levels. Their study is impressive and has reference value for future use of NIR spectroscopy. However, several issues can be highlighted, such as small-signal band shifts on the

91 collected NIR spectra; e.g., a sample strain of 0.1% would induce a band shift of
92 approximately 2 cm^{-1} at around 6470 cm^{-1} (3OH···5O). Moreover, since the molecules
93 are influenced by neighboring molecules, actuarial peaks overlap on the NIR spectra
94 (Okazaki 2012). Indeed, advanced curve fitting approaches could be used to predict the
95 peak shift, but the band shift varies among specimens, which has been confirmed by the
96 IR method (Eichhorn 2001). The spectral information of such long-wave sensitive
97 spectrometers is rather rich, and, as such, it requires expensive equipment, such as
98 detectors and light sources (Xing et al. 2008). Accordingly, there is still room to develop
99 and improve NIR spectra collection and data analyisis methods, expecially for practical
100 application purposes .
101
102 The most likely to be neglected is that bulk wood is a highly scattering medium, and
103 the light scattering degree inside the wood cell wall also highly correlates with the
104 microstructur (Ban et al. 2018; Ma et al. 2018a, 2019). Studies show that the reduced light
105 scattering coefficient ($\mu_s' = 10 - 100\ cm^{-1}$) is much larger than the absorption
106 coefficient ($\mu_a = 0.05 - 1.00\ cm^{-1}$) in the wavelength range of 700-1040 nm for both
107 softwood and hardwood species treated in different ways (dry, wet and degraded)
108 (D'Andrea et al. 2007). The deformation under longitudinal tension includes

109 macromolecule deformations in the layers and interlaminar slippages. The former is
110 related to the structure, orientation, and interaction of the polymers in the wood, and the
111 latter slippage deformation results from the structural differences between cell-wall layers
112 (Keckes et al. 2003; Adler and Buehler 2013). The misalignment between the cellulose
113 fibrils to the strain direction is amplified by bending and shearing of anatomical structures
114 and straightening of slightly waved cellulose microfibrils, forming lenticular spaces
115 between adjacent fibrils (Salmén 2015). The weak interfaces of wood cells or annual rings
116 could deflect transverse cracks into the longitudinal plane (Smith et al. 2003; Marthin and
117 Kristofer Gamstedt 2019; Guo et al. 2020). Hence, effective utilization of the light
118 scattering degrees (i.e., microstructure changs) inside the wood during tension testing
119 should predict strain levels accurately. This method also can reduce costs associated with
120 equipment because shorter wavelengths are scattered more strongly than longer
121 wavelengths in the visible (Vis)–NIR optical range (Ma et al. 2018a).
122
123 However, conventional Vis–NIR spectrometry acquires spectral data from a single
124 sample point based on the collective effects of light absorption (due to chemical
125 components such as water and cellulose content) and scattering (due to physical structures
126 such as cell size and intercellular spacing) (Vanoli et al. 2020). Studies have mainly relied

127 on performing further spectral pretreatments, such as baseline offset correction or
128 standard normal variate (SNV), that reduce light scattering effects before training
129 calibration models (Zude et al. 2011). Spatially resolved spectroscopy (SRS) requires
130 relatively strong, steady-state spotlights for illumination, and its diffusely reflected light
131 pattern is collected at multiple distances for light absorption and scattering evaluation
132 (Farrell et al. 1992; Qin et al. 2009; Lu et al. 2020). SRS has two main measurement
133 configurations: spectral imaging and fiber probing. On the one hand, the SRS based on
134 spectral imaging is a non-contact method that measures spatially resolved diffuse
135 reflectance over a broad spectral range (Peng and Lu 2008; Qin and Lu 2008; Zhu et al.
136 2015). The measurement system mainly consists of a hyperspectral imaging (HSI) camera,
137 a prime lens, and a small broadband beam as illumination. However, the light beam and
138 source-detector distance need to be carefully considered in this configuration, as they
139 determine the measured results (Cen and Lu 2010; Lu et al. 2020). On the other hand, the
140 fiber probe-based SRS is a contact method, which is often inconvenient for rapid online
141 quality assessment (Ma et al. 2018a). However, due to the easy-to-operate design with a
142 strong light reflectance, fiber probe-based SRS portable systems are desirable alternatives
143 for on-site applications. Besides, contact methods are more suitable to predict the strains
144 of moving wood sampels caused by tension testing than non-contact methods.

This paper reports on wood strain prediction results obtained by evaluating the changes in Vis–NIR SRS spectral data collected from wood samples during tension testing. The objectives of this paper are as follows: (1) design a multifiber-based Vis–NIR SRS system to rapidly and nondestructively acquire light scattering characteristics; (2) examine the relationship between SRS signals and wood tension strains by principal component analysis (PCA); and (3) construct wood strain calibration models by partial least squares (PLS) regression. This study should provide new insights into SRS methods for practical application to predict the tensile strain of wood conveniently and cost-effectively.

2. Materials and methods

2.1 Sample preparation

Wood samples (*Hinoki cypress*) with a length of 120 mm (longitudinal), a width of 10 mm (radial), and various thicknesses (tangential: 2 mm, 3 mm, 4 mm, and 5 mm) were sawn from air-dried wood board commercially purchased from a local wood processing company. Specimens were selected from mature wood parts sufficiently far from the pith to neglect ring curvature.

For the preliminary experiment, samples with different thicknesses (2 mm, 3 mm, 4 mm, and 5 mm) were measeud to evaluate the influence of thickness. Then, for the

primary experiment, 18 wood samples with the same thickness (2 mm) were tested to construct a strain calibration model. The samples were selected based on the wood fiber directions, which were as parallel as possible to the longitudinal direction. Before the experiment, all the samples remained in a desiccator, where relative humidity (RH) was controlled at 59% with a saturated salt solution of sodium bromide. Subsequently, the sample weights were measured for the equilibrated specimens using a digital balance (accuracy of 0.0001 g). A digital caliper (0.01 mm accuracy) measured the sample dimensions under the equilibrated condition. From the measured weights and dimensions of the raw data, sample equilibrium moisture content (EMC) and density were calculated according to the following equations:

$$\mathrm{EMC}(\%) = \frac{W - W_d}{W_d} \quad (1)$$

$$\mathrm{Density}\left(\frac{kg}{m^3}\right) = \left(\frac{W}{V}\right) \quad (2)$$

where W and W_d are weights for the equilibrated and oven-dried samples, respectively, and V is the sample volume under the equilibrated condition.

2.2 Tensile test

Each prepared wood sample was placed in a bending testing machine (preliminary experiment: Shimadzu AG-100KNI, Shimadzu, Japan; primary experiment: The SVZ-

50NA, IMADA-SS Corporation, Japan). During tension test, the bending machine was suspended several times manually to obtain strain measurements and Vis–NIR SRS data. The strain was recorded with strain gauges (FLAB-5-11, Tokyo Sokki Kenkyujo, Japan) glued to one side of each sample with instant adhesive (CN, Tokyo Sokki Kenkyujo, Japan) and connected to a strain-meter (TC-32K, Tokyo Sokki Kenkyujo, Japan). A Vis–NIR measurement system was used to collect light scattering characteristics on the other sample side (Fig. 1 (a) and (b)).

2.3 Visible and near-infrared spatially resolved spectroscopy measurements

Fig. 1 (c) and (d) show the measurement part (i.e. the fixator of light illumination and detection fibers) of the proposed Vis–NIR SRS system and a diagram of the internal structure. A 5-W halogen lamp initially provided light illumination. An optical fiber (SOG-70S, Sumita Optical Glass, Inc., Saitama, Japan) translated the light source onto each wood sample. Then, 30 silica fibers (Vis–NIR type, Core: 100 μm, Clad: 110 μm, Fiberguide Industries, New Jersey, USA) were separated into five groups (1, 2, 3, 4, and 5 from the light illumination point) to collect the diffuse reflected light and transfer it to the Vis–NIR HSI camera (SPECT-100nir1F, Spectral Application Research Laboratory Co., Ltd. Shizuoka, JAPAN). Inside the camera, the light beam was dispersed into spectral

components (vertical axis) while preserving spatial information (horizontal axis), and the camera took two-dimensional light signals. The shutter speed and framerate were set at 15 ms and 8 fps, respectively. In this study, the fixator was pasted parallelly to the sample grain direction with a double-sided tape, which was easily removable after measurement collection. The sensitive wavelength range of the Vis–NIR HSI camera was 600–1100 nm, with a minimum reading width of approximately 0.65 nm/pixel and a spectral resolution of 4.5 nm. For each measurement, 16 spectral images were captured and their averaged values saved. Light reference was measured using a tailor-made integrating sphere, i.e., a plastic ball (diameter of 6 cm) covered in barium sulfate. Dark values were measured by turning off the light and covering the light-collection fibers. Wavelengths under 660 nm and over 1002 nm were noisy and unreliable. Thus, a wavelength range of 660–1002 nm was selected for further data analysis. The collected spectra were then converted to the reflectance values by Eq. (3):

$$R_\lambda = \frac{S_\lambda - D_\lambda}{B_\lambda - D_\lambda} \quad (3)$$

where λ denotes the wavelength, S and B are the sample and a white reference spectrum, respectively, and D is the dark spectrum.

A desital camera took photos (16 × amplification) of another wood sample (thickness of 2 mm) before and after the tensile test to understand the submicroscopic changes during tension testing.

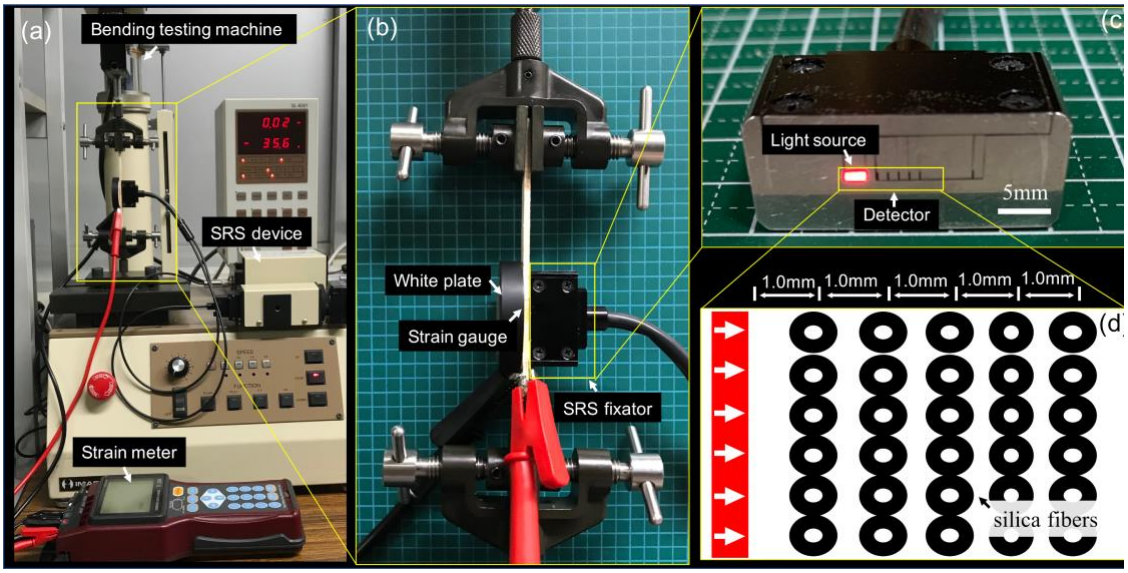

Fig. 1 (a) Experiment instruments; (b) Vis–NIR SRS data and strain measurements; (c) fixator of the Vis–NIR SRS measurement system; (d) internal structure diagram of the fixator.

2.4 Spectra pretreatments and principal component analysis

The Vis–NIR SRS spectra were smoothed by a Savitzky–Golay filter (polynomial order: 2; frame length: 15). The spectral data, collected before tension testing subtracted from various strain levels, were tested to correct the natural variability of physical structure among wood samples. Then, PCA with the mean center was used to “compress” the Vis–NIR spectral data to examine the correlation between measured strain reference values and the spectra data changes. It is noteworthy that no other spectra pretreatments

(e.g., SNV (Cuesta Sánchez et al. 1995) and the second derivative (Gorry 1991)) were used in this study to keep the maximum light scattering information.

2.5 Partial least squares regression analysis

The Vis–NIR difference spectral data were calibrated with the measured strain values via PLS regression (Martens and Tormod 1992). In developing the PLS regression models, 70 % of measured data was randomly selected as the calibration set, leaving 30 % for the test set. Five-fold cross-validation optimized the number of latent variables (LVs). The coefficients of determination *(R^2)* and the root mean squared error (RMSE) characterized the constructed calibration model's performance:

$$R^2 = 1 - \frac{\sum_{i=1}^{n}(y_i - \hat{y}_i)^2}{\sum_{i=1}^{n}(y_i - \bar{y})^2} \quad (4)$$

$$\mathrm{RMSE} = \sqrt{\frac{1}{n}\sum_{i=1}^{n}(\hat{y}_i - y_i)^2} \quad (5)$$

where n is the number of measurements, y is the reference strain values, $\hat{y}$ is the strain value predicted by PLS regression analysis, and $\bar{y}$ is the mean value of y.

Variable importance in projection (VIP) scores were used to identify the influence of the SRS spectral data collected by the individual fiber groups on the PLS model (Wold et al. 1993; Farrés et al. 2015). Data analysis was performed by MATLAB (The MathWorks Inc., Natick, MA).

3 Results and discussion

Fig. 2 shows the raw spectral image of a wood sample with a thickness of 2 mm taken by the Vis–NIR HSI camera before the tensile test. This image data contains the spatial information of the 30 silica fibers (horizontal axis) and the spectral information of the measured wood sample (vertical axis). The main difficulty with conventional SRS methods is associated with collecting the spectral data with a high signal-to-noise ratio quickly. One method involves repeating the same data measurements and averaging the results, which is time-consuming (Tkachenko 2006). This study is desirable for the spectral data acquisition time to be short of excluding additional relaxation phenomena (Burgert 2006; Altaner et al. 2014) This was achieved by a two-step signal averaging process: (i) each fiber occupies 34 pixels of the HSI camera, and the central 30 pixels were averaged for spectral data collection, after which (ii) the signals of six fibers in the same group were averaged.

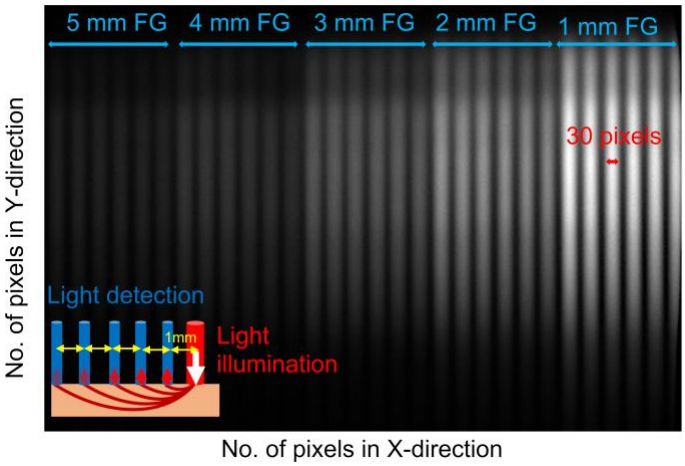

Fig. 2. Raw Vis–NIR SRS spectral image of wood sample with 2 mm thickness.

258

259 Fig. 3 shows the Vis–NIR SRS spectra with standard deviations of the 18 wood
260 samples at various tension levels, which were initially calculated from the raw spectral
261 image shown in Fig. 2. It is logical that the overall spectral intensity quickly falls with an
262 increase in distance from the light illumination. The wavelength at 925 nm corresponds
263 to the third overtone of C–H absorption (Mohammadi-Moghaddam et al. 2018), which
264 can be attributed to the chemical components of the wood samples. The wavelength at
265 approximately 930 nm has the highest light reflectance when the fiber group is 3–4 mm
266 away from the light illumination, suggesting that the light at said wavelength was less
267 absorbed and transmittted further from the light illumination than other wavelengths
268 along the wood grain direction. It is noteworthy that the optical scattering was not
269 isotropic within each wood sample; the light propagated further in the parallel direction

because the scattering coefficient along the cylinders is much smaller than that in the perpendicular direction to the cylinders (Ma et al. 2018b, 2019).

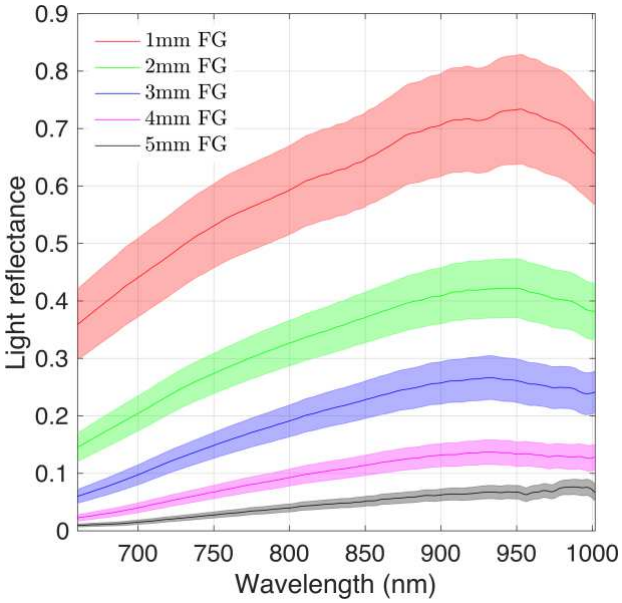

Fig. 3 Averaged Vis–NIR raw spectra and the standard deviations (light color) of 18 samples with the same thickness (2 mm) and various tension strains.

Fig. 4 shows the Vis–NIR spectral data for various strain measurements for wood samples with different thicknesses (vertical) by the five fiber groups (horizontal), respectively. The wavelength range was selected to 900–950 nm to expand the image size. The light reflectance increased with an increase in wood strain. Light absorption at 925 nm is the most obvious at the spectra collected by the 1-mm fiber group. The signal quality decreases with an increase in distance between the light illumination and light-detection fibers, suggesting that different fiber groups can collect spectral data with

different light absorption and scattering degrees. Light reflectance is also affected by sample thickness. The differences in the Vis–NIR spectral data, caused by sample strains, diminished in thicker samples, especially at far fiber groups. This could be due to the light transmission depth is different among the wood samples at various thicknesses. In this study, the Vis–NIR light was transmitted through hinoki wood samples with an approximate thickness of 5 mm (see the supplementary, Fig. S1), after which it was reflected by the white plate and detected by optical fibers. However, because thicker wood samples have a more profound light transmission, which affectted light propagating in parallel, stronger noise was associated with the collected spectra at more extended fiber groups. Except for signal quality, because the strain gauge was stuck on the opposite side of the SRS fixator, less transmission light could also reduce the correlation between SRS data and strain reference values. This suggests that the proposed SRS equipment is suitable for predicting the tension strain of wood sampels with an approximately of 2–3 mm. Further improvements could be useful to construct strain prediction models for thicker samples, such as reducing the distance between fiber groups and introducing a method to measure the strain changs where the spectral data were collected.

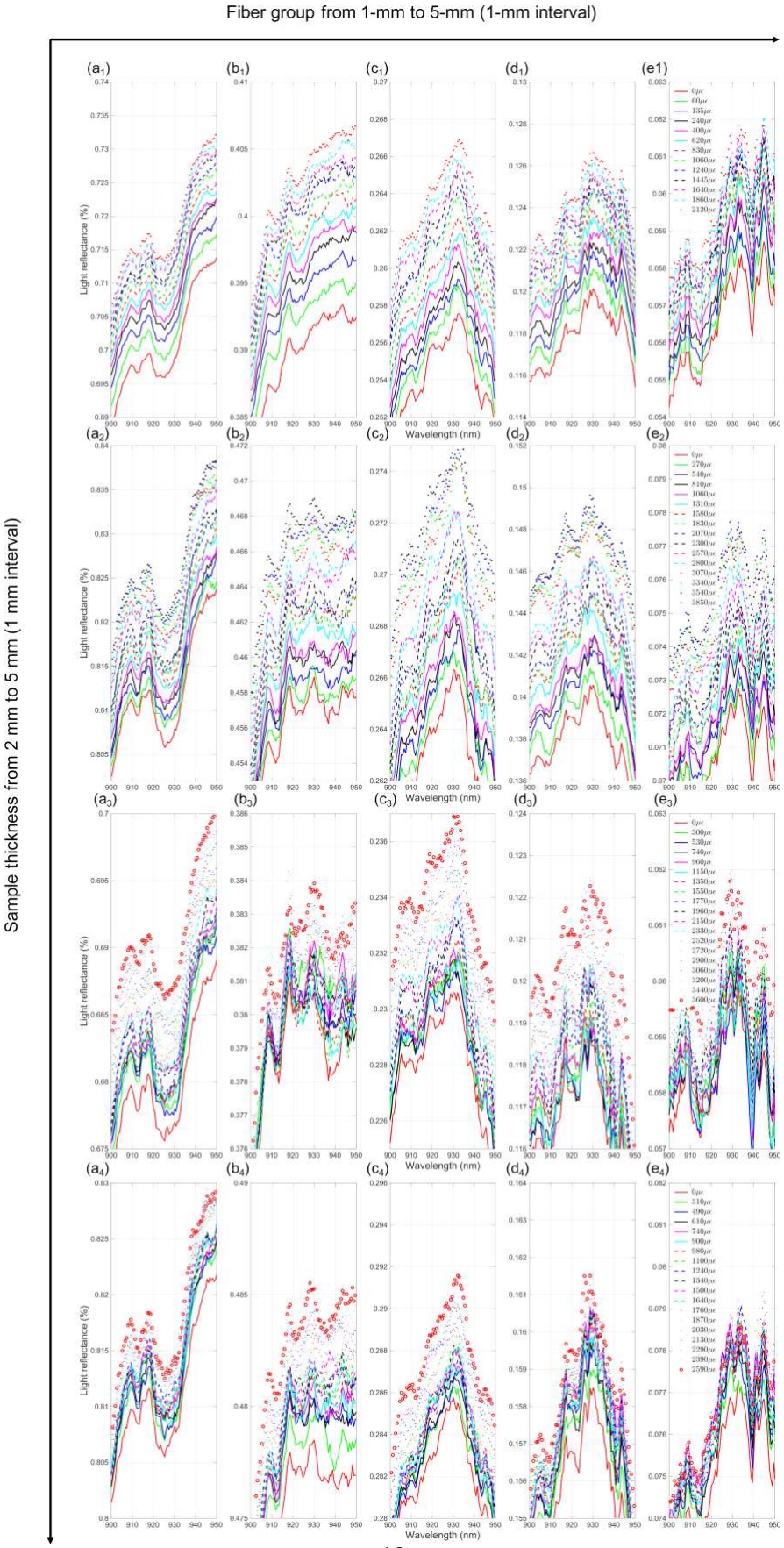
Fiber group from 1-mm to 5-mm (1-mm interval)
Sample thickness from 2 mm to 5 mm (1 mm interval)
Light reflectance (%)
Wavelength (nm)
(a1)
(b1)
(c1)
(d1)
(e1)
(a2)
(b2)
(c2)
(d2)
(e2)
(a3)
(b3)
(c3)
(d3)
(e3)
(a4)
(b4)
(c4)
(d4)
(e4)

Fig. 4 Vis–NIR SRS spectral data collected at various sample thicknesses (vertical) by different fiber groups (horizontal).

296

297 Fig. 5 (b) and (c) show the digital photos of wood samples before and after tension
298 testing with a strain of 3410 με. The stretched wood cell wall could decrease the density
299 of the measured area and increases the aperture on the cell wall between the light source
300 and the five fiber groups of the SRS fixator. Hence, the light reflectance values increased
301 during the tension test.

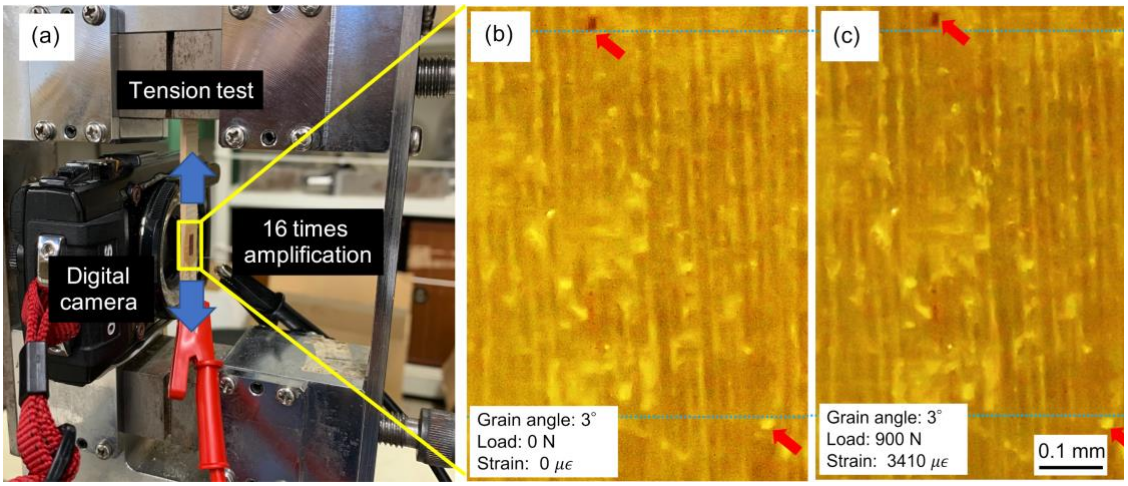

Fig. 5 Digital photos of the wood sample with 2 mm thickness before (a) and after (b) the tension test, respectively.

302

303 The spectral data collected from the five fiber groups at a wavelength range of 660–
304 1002 nm were concatenated, resulting in 2555 variance values (Figure 6 ($a_{1\text{-}4}$)). Fig. 6
305 ($b_{1\text{-}4}$)) shows the first two principal component (PC) loadings. The PC loadings can be
306 understood as the weights for each variance value when calculating the PC score. The

307 accumulated contribution rate of the frist two scores is approximately 99.64%, 99.15%,
308 97.47%, and 94.48% for a sample thickness of 2, 3, 4, and 5 mm, respectively. The PC1
309 and PC2 scores of the SRS are shown in Fig. 6 ($c_{1\text{-}4}$), where the Y-axis shows PC2 and
310 the X-axis shows the PC1. There is a strong correlation between PC1 loading and light
311 scattering differences, i.e., vertical baseline shift. As expected from Fig. 4, the
312 contribution rate of the PC 1 score decreases with an increase in sample thickness.
313 Moreover, PC2 loading has relatively high absolute values at a light wavelength of 970
314 nm. This suggests a meaningful correlation between the light absorption by hydrogen
315 bonds and wood strain changings, but the contribution rate was much lower than the light
316 scattering differences.

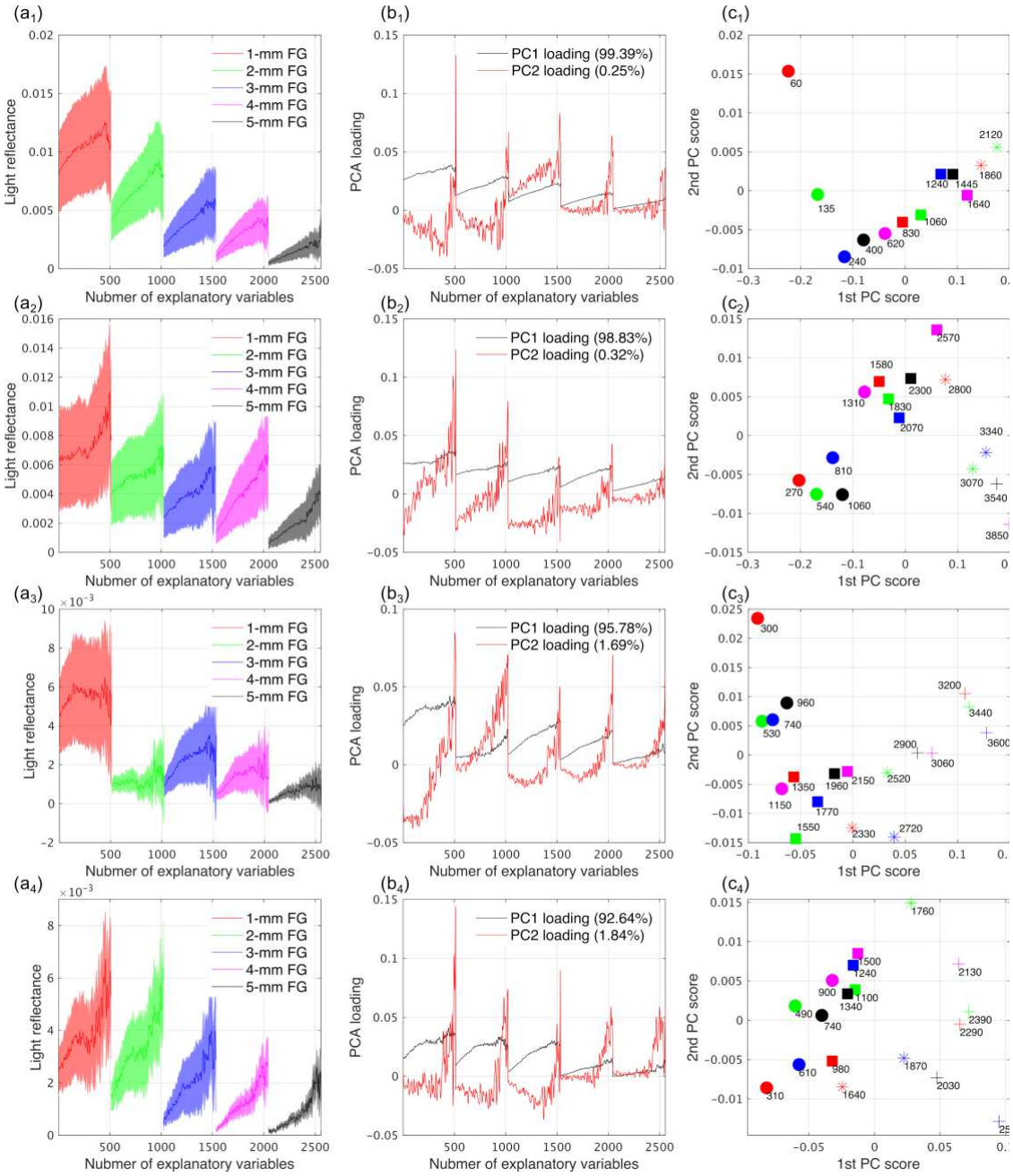

Fig. 6 (a_{1-4}) Concatenated Vis-NIR difference spectral data used for PCA; (b_{1-4}) first two principal component loadings; (c_{1-4}) first two principla component scores of the concatenated Vis-NIR spectral data.

317

318 Fig. 7 (a) shows the strain calibration results of the wood samples with the same

319 thickness (2 mm) from the PLS regression method with LV numbers 9 (explanatory

variables: Vis-NIR difference spectral data after pretreatments; response variables: strain reference values). The density of the samples was 415 ± 14 kg/m^3 and the MC was $10.51\% \pm 0.26\%$. Overall, the PLS calibration model has a high prediction accuracy: the R^2 and RMSE of the calibration set are 0.86 and 297.89 με, respectively. For the validation set, the R^2 and RMSE are 0.82 and 345.44 με, respectively. Differences in the RMSE can be attributed to the fact that the strain gauge only measured the surface strain of each wood sample, whereas the SRS method measured the whole strain with the information of sample thickness. Indeed, there is a possibility that the SRS method can more accurately measure the wood sample strain than conventional strain gauges, but further studies are required to prove this. Overall, this is the first study to suggest that the Vis–NIR SRS method combined with PLS regression analysis can predict the tensile of wood samples with the same thickness (also see the prediction results of the wood samples with the same 5 mm thickness in supplementary, Fig. S2). Fig. 7 (b) shows the strain calibration results when using the raw Vis–NIR spectral data, it is evident that the difference spectral data could be used to achieve the initial value correction purpose , thus are necessary to construct the strain calibration model.

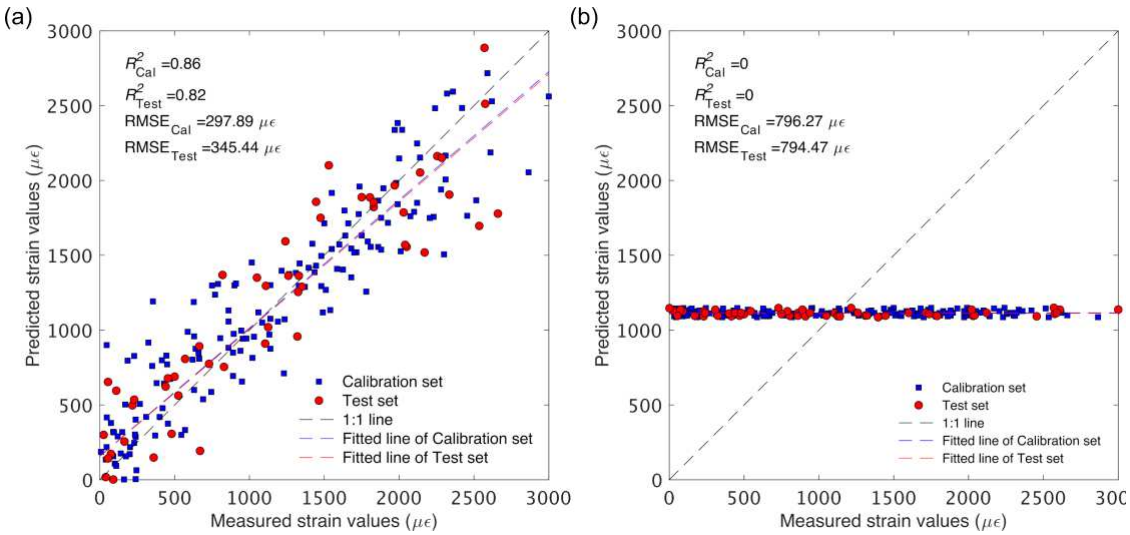

Fig. 7 Scatter plot of measured and predicted strain values using (a) difference spectral data or (b) raw spectral data.

337

338 Fig. 8 (a) shows the VIP scores, from which it is evident that the number of important
339 wavelengths (VIP scores>1) decreased with an increase in distance between light
340 detection and illumination. Fig. 8(b) shows the PLS regression coefficients regarding
341 the Vis–NIR difference spectra. It was somewhat surprising that although the contribution
342 rate calculated by PCA at the wavelengths related to the hydrogen bonds is much lower
343 than the light scattering differences at each sample, it is important to constract a strain
344 calibration model using all 18 samples. It could be supportted by the knowledge that wood
345 becomes more ductile with increased MC (Ozyhar et al. 2012; Mvondo et al. 2017) which
346 also affects the light scattering degree (Konagaya et al. 2016). This also suggests that MC
347 effects much be fully valued, to build individual calibration models depends on sample
348 MC may be the best way to reduce the MC effects.

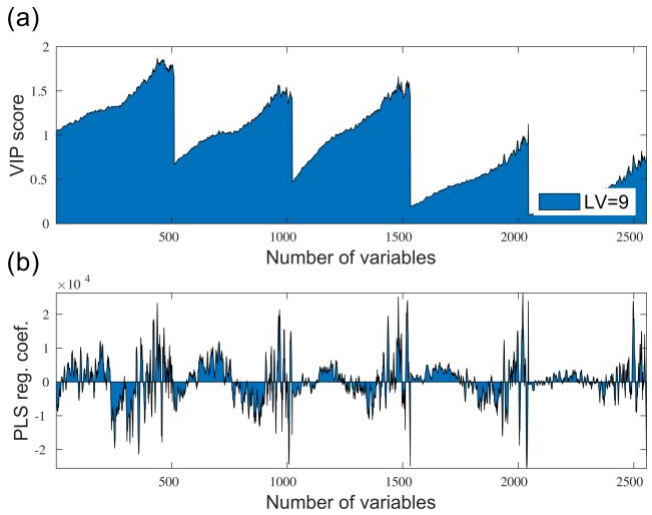

Fig. 8 (a) VIP scores of the SRS spectral data; (d) PLS regression coefficients.

4 Conclusion

This study aims to demonstrate the correlation between light scattering changes inside the wood cell walls and tensile strain. Spatially resolved diffuse reflectance was collected by designing a portable and cost-effective measurement system based on fiber probes. For the preliminary experiment, samples with different thicknesses (2 mm, 3 mm, 4 mm, and 5 mm) were measured to evaluate the influence of thickness. Then, for the primary experiment, 18 wood samples with the same thickness (2 mm) were tested to construct a strain calibration model. The prediction accuracies were characterized by an R^2 of 0.86 and an RMSE for 297.89 με for five-fold cross-validation, 0.82 and 345.44 μ for test validation. The designed SRS measurement system does not require sophisticated measurement techniques. Moreover, it has a cost design effective design due to the Vis–

NIR HSI camera with short-wave sensitivity, which is much cheaper than long-wave sensitivity cameras.

Further research should focus on extending the applicability of the SRS approach to a broader database of wood types and larger sample numbers with various thicknesses. The intervals between fiber groups could be changed to test the strain predicion of thicker wood samples. This research also references further research to measure growth strain in trees non-destructively. However, because light scattering degree is also affected by MC, this would require more in-depth spectral pretreatments.

5 Acknowledgments

The authors are grateful for the financial support provided by JSPS (KAKENHI, no.19K15886)

6 References

Adler DC, Buehler MJ (2013) Mesoscale mechanics of wood cell walls under axial strain. Soft Matter 9:7138–7144. https://doi.org/10.1039/c3sm50183c

Åkerholm M, Salmén L (2001) Interactions between wood polymers studied by dynamic FT-IR spectroscopy. Polymer (Guildf) 42:963–969.

https://doi.org/10.1016/S0032-3861(00)00434-1

Altaner CM, Thomas LH, Fernandes AN, Jarvis MC (2014) How cellulose stretches: Synergism between covalent and hydrogen bonding. Biomacromolecules 15:791–798. https://doi.org/10.1021/bm401616n

Anaf W, Cabal A, Robbe M, Schalm O (2020) Real-time wood behaviour: The use of strain gauges for preventive conservation applications. Sensors (Switzerland) 20:. https://doi.org/10.3390/s20010305

Baillères H, Hopewell G, Boughton G, Brancheriau L (2012) Strength and stiffness assessment technologies for improving grading effectiveness of radiata pine wood. BioResources 7:1264–1282. https://doi.org/10.15376/biores.7.1.1264-1282

Ban M, Inagaki T, Ma T, Tsuchikawa S (2018) Effect of cellular structure on the optical properties of wood. J Near Infrared Spectrosc 26:53–60. https://doi.org/10.1177/0967033518757233

Barr AD, Clarke SD, Tyas A, Warren JA (2017) Electromagnetic Interference in Measurements of Radial Stress During Split Hopkinson Pressure Bar Experiments. Exp Mech 57:813–817. https://doi.org/10.1007/s11340-017-0280-4

Burgert I (2006) Exploring the Micromechanical Design of Plant Cell Walls. Am J Bot 93:1391–1401

Cen H, Lu R (2010) Optimization of the hyperspectral imaging-based spatially-resolved system for measuring the optical properties of biological materials. Opt Express 18:17412. https://doi.org/10.1364/oe.18.017412

Cuesta Sánchez F, Toft J, van den Bogaert B, et al (1995) Monitoring powder blending by NIR spectroscopy. Fresenius J Anal Chem 352:771–778. https://doi.org/10.1007/BF00323062

D'Andrea C, Farina A, Comelli D, et al (2007) Time-resolved diffuse optical spectroscopy of wood. Opt InfoBase Conf Pap 62:569–574. https://doi.org/10.1117/12.727955

Eichhorn YRJ (2001) The young's modulus of a microcrystalline cellulose. Cellulose 8:197–207. https://doi.org/10.1023/A:1013181804540

Farrell TJ, Patterson MS, Brain W (1992) A diffusion theory model of spatially resolved, steady-state diffuse reflectance for the noninvasive determination of tissue optical properties in vivo. Medphys 19:879–888. https://doi.org/10.1118/1.596777

Farrés M, Platikanov S, Tsakovski S, Tauler R (2015) Comparison of the variable importance in projection (VIP) and of the selectivity ratio (SR) methods for variable selection and interpretation. J Chemom 29:528–536.

https://doi.org/10.1002/cem.2736

Gorry PA (1991) General Least-Squares Smoothing and Differentiation of Nonuniformly Spaced Data by the Convolution Method. Anal Chem 63:534–536. https://doi.org/10.1021/ac00005a031

Guo F, Altaner CM (2018) Molecular deformation of wood and cellulose studied by near infrared spectroscopy. Carbohydr Polym 197:1–8. https://doi.org/10.1016/j.carbpol.2018.05.064

Guo F, Altaner CM, Jarvis MC (2020) Thickness-dependent stiffness of wood: Potential mechanisms and implications. Holzforschung 74:1079–1087. https://doi.org/10.1515/hf-2019-0311

Guo F, Cramer M, Altaner CM (2019) Evaluation of near infrared spectroscopy to non-destructively measure growth strain in trees. Cellulose 26:7663–7673. https://doi.org/10.1007/s10570-019-02627-2

Hon DNS, Chang ST (1984) Surface Degradation of Wood By Ultraviolet Light. J Polym Sci A1 22:2227–2241. https://doi.org/10.1002/pol.1984.170220923

Hsieh YC, Yano H, Nogi M, Eichhorn SJ (2008) An estimation of the Young's modulus of bacterial cellulose filaments. Cellulose 15:507–513. https://doi.org/10.1007/s10570-008-9206-8

433 Kamiyama T, Suzuki H, Sugiyama J (2005) Studies of the structural change during
434 deformation in Cryptomeria japonica by time-resolved synchrotron small-angle X-
435 ray scattering. J Struct Biol 151:1–11. https://doi.org/10.1016/j.jsb.2005.04.007
436 Keckes J, Burgert I, Frühmann K, et al (2003) Cell-wall recovery after irreversible
437 deformation of wood. Nat Mater 2:810–814. https://doi.org/10.1038/nmat1019
438 Konagaya K, Inagaki T, Kitamura R, Tsuchikawa S (2016) Optical properties of drying
439 wood studied by time-resolved near-infrared spectroscopy. Opt Express 24:9561.
440 https://doi.org/10.1364/OE.24.009561
441 Liu Q, Ding W, Zhou H, et al (2015) A Novel Strain Measurement System in Strong
442 Electromagnetic Field. IEEE Trans Plasma Sci 43:3562–3567.
443 https://doi.org/10.1109/TPS.2015.2418276
444 Lu R, Van Beers R, Saeys W, et al (2020) Measurement of optical properties of fruits
445 and vegetables: A review. Postharvest Biol Technol 159:111003.
446 https://doi.org/10.1016/j.postharvbio.2019.111003
447 Ma T, Inagaki T, Tsuchikawa S (2019) Three-dimensional grain angle measurement of
448 softwood (Hinoki cypress) using near infrared spatially and spectrally resolved
449 imaging (NIR-SSRI). Holzforschung 73:817–826. https://doi.org/10.1515/hf-2018-
450 0273

Ma T, Schajer G, Inagaki T, et al (2018a) Optical characteristics of Douglas fir at various densities, grain directions and thicknesses investigated by near-infrared spatially resolved spectroscopy (NIR-SRS). Holzforschung 1–8. https://doi.org/10.1515/hf-2017-0213

Ma T, Schajer G, Inagaki T, et al (2018b) Optical characteristics of Douglas fir at various densities, grain directions and thicknesses investigated by near-infrared spatially resolved spectroscopy (NIR-SRS). Holzforschung 72:789–796. https://doi.org/10.1515/hf-2017-0213

Ma T, Tsuchikawa S, Inagaki T (2020) Rapid and non-destructive seed viability prediction using near-infrared hyperspectral imaging coupled with a deep learning approach. Comput Electron Agric 177:. https://doi.org/10.1016/j.compag.2020.105683

Martens H, Tormod N (1992) Multivariate calibration. John Wiley & Sons.

Marthin O, Kristofer Gamstedt E (2019) Damage shielding mechanisms in hierarchical composites in nature with potential for design of tougher structural materials. R Soc Open Sci 6:. https://doi.org/10.1098/rsos.181733

Mohammadi-Moghaddam T, Razavi SMA, Sazgarnia A, Taghizadeh M (2018) Predicting the moisture content and textural characteristics of roasted pistachio

469 kernels using Vis/NIR reflectance spectroscopy and PLSR analysis. J Food Meas
470 Charact 12:346–355. https://doi.org/10.1007/s11694-017-9646-7
471 Montero C, Clair B, Alméras T, et al (2012) Relationship between wood elastic strain
472 under bending and cellulose crystal strain. Compos Sci Technol 72:175–181.
473 https://doi.org/10.1016/j.compscitech.2011.10.014
474 Mvondo RRN, Meukam P, Jeong J, et al (2017) Influence of water content on the
475 mechanical and chemical properties of tropical wood species. Results Phys
476 7:2096–2103. https://doi.org/10.1016/j.rinp.2017.06.025
477 Okazaki Y (2012) Near-Infrared Spectroscopy—Its Versatility in Analytical. Anal
478 Chem 28:545–562
479 Ozyhar T, Hering S, Niemz P (2012) Moisture-dependent elastic and strength
480 anisotropy of European beech wood in tension. J Mater Sci 47:6141–6150.
481 https://doi.org/10.1007/s10853-012-6534-8
482 Peng Y, Lu R (2008) Analysis of spatially resolved hyperspectral scattering images for
483 assessing apple fruit firmness and soluble solids content. Postharvest Biol Technol
484 48:52–62. https://doi.org/10.1016/j.postharvbio.2007.09.019
485 Peura M, Kölln K, Grotkopp I, et al (2007) The effect of axial strain on crystalline
486 cellulose in Norway spruce. Wood Sci Technol 41:565–583.

https://doi.org/10.1007/s00226-007-0141-x

Qin J, Lu R (2008) Measurement of the optical properties of fruits and vegetables using spatially resolved hyperspectral diffuse reflectance imaging technique. Postharvest Biol Technol 49:355–365. https://doi.org/10.1016/j.postharvbio.2008.03.010

Qin J, Lu R, Peng Y (2009) Prediction of apple internal quality using spectral absorption and scattering properties. Trans ASABE 52:486–499. https://doi.org/10.13031/2013.26807

Salmén L (2015) Wood morphology and properties from molecular perspectives. Ann For Sci 72:679–684. https://doi.org/10.1007/s13595-014-0403-3

Salmén L, Bergström E (2009) Cellulose structural arrangement in relation to spectral changes in tensile loading FTIR. Cellulose 16:975–982. https://doi.org/10.1007/s10570-009-9331-z

Smith I, Landis E, Gong M (2003) Fracture and fatigue in wood. John Wiley & Sons

Tkachenko N V (2006) Chapter 7 - Flash–photolysis. In: Optical Spectroscopy. Elsevier Science, Amsterdam, pp 129–149

Vanoli M, Van Beers R, Sadar N, et al (2020) Time- and spatially-resolved spectroscopy to determine the bulk optical properties of ‘Braeburn’ apples after ripening in shelf life. Postharvest Biol Technol 168:.

505 https://doi.org/10.1016/j.postharvbio.2020.111233
506 Wold S, Johansson E, Cocchi M (1993) PLS: partial least squares projections to latent
507 structures
508 Xing Z, Wang J, Shen G (2008) Short-Wave Near-Infrared Spectroscopy for Rapid
509 Quantification of Acidity of Aviation Kerosene. Open Fuels Energy Sci J 1:51–53.
510 https://doi.org/10.2174/1876973x00801010051
511 Yang JL, Baillères H, Okuyama T, et al (2005) Measurement methods for longitudinal
512 surface strain in trees: A review. Aust For 68:34–43.
513 https://doi.org/10.1080/00049158.2005.10676224
514 Yu Y, Jiang Z, Tian G (2009) Size effect on longitudinal MOE of microtomed wood
515 sections and relevant theoretical explanation. For Stud China 11:243.
516 https://doi.org/10.1007/s11632-009-0040-3
517 Zhu Q, He C, Lu R, et al (2015) Ripeness evaluation of “Sun Bright” tomato using
518 optical absorption and scattering properties. Postharvest Biol Technol 103:27–34.
519 https://doi.org/10.1016/j.postharvbio.2015.02.007
520 Zude M, Pflanz M, Spinelli L, et al (2011) Non-destructive analysis of anthocyanins in
521 cherries by means of Lambert-Beer and multivariate regression based on
522 spectroscopy and scatter correction using time-resolved analysis. J Food Eng

523 103:68–75. https://doi.org/10.1016/j.jfoodeng.2010.09.021

524

Supplementary Files

This is a list of supplementary files associated with this preprint. Click to download.

- Supplementary20210524.pdf